Recent progress in surface NMR-electrochemistry

Jianjun Wu,[a] James B. Day,[a] Krzysztof Franaszczuk,†[a] Bernard Montez,[a] Eric Oldfield,[a]* Andrzej Wieckowski,[a]* Pierre-André Vuissoz[b] and Jean-Philippe Ansermet[b]*

[a] *Department of Chemistry, University of Illinois at Urbana-Champaign, 505 South Mathews Avenue, Urbana, Illinois 61801, USA and Frederick Seitz Materials Research Laboratory, University of Illinois at Urbana-Champaign, 104 South Goodwin Avenue, Urbana, Illinois 61801, USA*

[b] *École Polytechnique Fédérale de Lausanne, Institut de Physique Expérimentale, CH-1015 Lausanne, Switzerland*

NMR spectroscopy is one of the newer spectroscopic techniques for investigating the static, dynamic and electronic structures of molecules adsorbed onto metal catalyst surfaces. We review recent progress in the application of solid-state NMR methods to the investigation of molecules adsorbed onto metal surfaces in an electrochemical environment: in the presence of electrolyte, and at an electrified interface under external potentiostatic control. While at a very early stage of development, the NMR-electrochemistry approach has considerable potential for investigating otherwise inaccessible aspects of electrode and adsorbate structure, and should enable a comparison of results obtained from different spectroscopies, in particular from IR spectroscopy. We present a brief review of the development of the subject, followed by details of the instrumentation necessary for NMR-electrochemistry studies. We show how spin–spin relaxation can give information on surface structure and surface diffusion, how spin–lattice relaxation can give information on the presence of conduction electron spillover onto the adsorbate, and how the NMR of surface species responds to an externally applied electric field. The ^{13}C-NMR of CO on Pt in an electrochemical environment is compared with the ^{13}C-NMR of CO on Pt catalysts in vacuum, which are well characterized. In the case of CN on Pt, we show large spectral shifts of the resonance as the electrode potential is varied, providing an independent measurement of the effects of the electrified interface on the chemisorption bond. Spectral sensitivity is also now adequate to observe nuclei which produce even weaker signals than ^{13}C, such as ^{15}N. The NMR-electrochemistry method thus opens up a broad new array of possibilities for probing static structures (from T_2), surface diffusion (from the temperature dependence of T_2) as well as electronic properties of the chemisorption bond (from T_1, and from electrode potential effects) at electrochemical interfaces, and for studying reactive intermediates and poisons on high-surface-area catalysts, such as those utilized in hydrogen and organic fuel cells.

Solid-state NMR spectroscopy[1] can, in principle, provide considerable new insights into problems of importance in electrochemical surface science and catalysis such as: (i) the nature of the surface chemical bond and the local surface density of states; (ii) the intramolecular structure of adsorbates; (iii) distances between adsorbates and (iv) intra- and inter-molecular motions of adsorbates (*e.g.* surface diffusion). Unfortunately, NMR is a very low sensitivity technique, a problem which tends to be exacerbated in samples of metallic powders (where the radiofrequency has difficulty penetrating a sample owing to skin-depth effects). Further difficulty may arise if a sample is connected to an external device such as a potentiostat, where noise can be readily picked up from the local environment.

To illustrate the general difficulty of applying NMR to surface investigations, consider the fact that 1 cm^2 of a metal surface contains *ca.* 10^{15} atomic sites, while a typical NMR experiment (for ^{13}C) requires *ca.* 10^{19} spins.[2,3] Assuming a complete 1 : 1 adsorbate/metal coverage, this demands *ca.* 1 m^2 of a surface. One is, therefore, usually compelled to work with relatively large-surface-area samples, such as small metal particles supported on non-conducting substrates, such as η-alumina, silica, or titania. However, the requirements for an electrochemical sample differ significantly from those which are typically found for gas-phase heterogeneous catalysis studies. For electrochemistry, the sample must be an electrical conductor, and it should be at equipotential throughout its volume. With these *caveats* in mind, we first consider what might be learned if one could in fact carry out NMR experiments in an electrochemical environment. Then, we show that such experiments can indeed now be carried out.

Surface NMR investigations of selected gas-phase adsorbates

We review below, surface NMR data on some selected adsorbates obtained from the gas phase, that have a direct relevance to species studied at the solid/liquid interface, particularly surface CO, but also hydrogen, ethylene and acetylene. Work on adsorbed hydrogen started early on when the substrate was first palladium,[4] then later platinum, copper and tungsten.[5–7] While these very early studies dealt predominately with physisorption (see the review by Pfeifer[8]), more recent investigations have been concerned with chemisorbed species (for reviews see ref. 2, 3 and 9–12). The adsorption of carbon monoxide has been of particular interest, and has been widely investigated in materials such as rhodium supported on alumina,[13] ruthenium, rhodium and palladium supported on silica,[14–17] and platinum and palladium on alumina.[18–22] Two forms of surface CO, both well known in ultra-high vacuum (UHV) surface research, have been detected by NMR: linear- and bridge-bonded CO, as well as in some cases isolated metal carbonyls.[14] More detailed studies have enabled considerable structural information to be obtained, such as: C—O bond distances,[22] the local packing density of CO on metal particle surfaces,[18] as well as the rates of CO surface diffusion,[15,16,22] for example.

† Present address: Lyntech, Inc., 7610 Eastmark Drive, Suite 105, College Station, TX 77840, USA.

High resolution NMR has been attempted using magic angle sample spinning (MAS) of CO on silica-supported ruthenium and rhodium samples,[23] and has revealed isotropic shifts for the linearly bonded CO, but failed to detect narrow lines corresponding to bridge-bonded CO. This was attributed to an inherent heterogeneity of the bridge-bonded site. The lack of the MAS narrowing of ^{13}CO NMR spectra on alumina-supported platinum and palladium[24] has also been noted, and has been attributed to the heterogeneity of the CO adsorption site, as well as more complex problems associated with the large magnetic susceptibility of Pt. Thus, while magic angle sample spinning techniques are quite routinely used to investigate *e.g.* organic solids or metal carbonyls, they have been less successful in generating high-resolution NMR spectra of molecules adsorbed to metal (especially platinum) surfaces. On the one hand, this is unfortunate but, on the other, one is freed from the necessity of spinning a metallic sample in a magnetic field, while attached to a potentiostat, since clearly much useful information can be obtained by use of stationary samples.

Such solid-state NMR studies have also provided considerable information about the molecular structure of some other adsorbates. For example, acetylene adsorbed on supported platinum, osmium and iridium has been intensively studied.[25–27] Slichter and co-workers[26] investigated low levels of acetylene on alumina-supported Pt using spin-echo double resonance and multiple-quantum coherence techniques and concluded that, at low coverage and at room temperature, the main surface species was $\rangle C{=}CH_2$, with a bond length of 1.44 Å, midway between a single and a double bond. At high coverage, ethylidine was the main surface product,[27] in agreement with previous UHV work (ref. 28 and references therein). At high temperature, the C—C scission in ethylene and acetylene was shown to occur *via* different intermediates, but with very similar activation energies.

These investigations of metal–adsorbate interactions in gas-phase systems using static samples have resulted in many important observations relating to the static, dynamic, as well as the electronic structures of molecules adsorbed to metal surfaces, and they prompted us to try to extend these types of studies to an electrochemical environment.[29–31] The motivation for this research was simply to be able to merge electrochemical techniques with the familiar solid-state NMR armamentarium, enabling, in principle, all the typical types of solid/gas-phase NMR experiments, T_1, T_2, $T_1\rho$, diffusion, but at electrified interfaces, under potential control. Of course, other spectroscopies offer important alternative probes of surface structure in an electrochemical environment, but processes such as surface diffusion, thermodynamic properties, densities of states, as well as geometric properties such as bond lengths, are often difficult to determine using IR or scattering techniques and, at least, it was thought that the NMR-electrochemistry method should be a useful complementary technique—certainly one which might be very valuable for investigating real world electrocatalyst samples.

It was however, necessary to overcome the following major problems.

(1) Measurements were to be carried out with self-supported metal powder electrodes, precluding the standard high-temperature cleaning procedure used with supported metal catalysts.

(2) Conducting liquid (supporting electrolyte) was always to be present.

(3) A three-electrode electrochemical cell, operating in the NMR probe, was desirable.

(4) Radiofrequency pickup introduced into the probe by the potentiostat leads needed to be eliminated.

Fortunately, none of these problems produced insurmountable obstacles to obtaining NMR spectra, and recent instrumentation improvements, which are described below, provide greatly enhanced sensitivity, enabling detailed relaxation experiments to be performed.

Electrochemical NMR

Sealed samples

The first surface investigated by NMR-electrochemistry[29] involved the use of *ca.* 1 g of platinum, corresponding to *ca.* 20 m^2 of platinum surface area. The electrochemical adsorption and voltammetry characterization of such a sample is described in the following section. The particles, 80 Å on average,[31] were coalesced into micrometre-sized aggregates. This collection of electrically connected platinum microparticles exhibited voltammograms characteristic of a polycrystalline platinum electrode. The CO adsorbate was generated from 99% ^{13}C-enriched methanol decomposed on the platinum electrode in a preparative electrochemical cell.[29] The platinum powder, covered by the ^{13}C adsorbate, as well as the solution containing ^{13}C-enriched methanol, was then quickly transferred to an NMR tube (1.0 cm in diameter and 1.8 cm in length) and flame sealed under an inert gas atmosphere. Fig. 1 shows the ^{13}C NMR spectrum of such a PtCO (ads) sample.[29] Background samples containing platinum black powder in direct contact with clean electrolyte (0.5 M H_2SO_4, without any methanol) provided featureless baselines. The sharp peak at *ca.* 50 ppm downfield from tetramethylsilane (TMS) is due to methanol in solution, while the broad spectral feature centred at *ca.* 340–375 ppm downfield from TMS is characteristic of the ^{13}C surface product of methanol oxidation, PtCO(ads).

NMR samples with potential control

After these initial observations in a sealed sample, Slezak and Wieckowski constructed the first NMR electrochemical cell,[31,32] Fig. 2. The electrode was fabricated with a 7 mm glass frit and had a reservoir for the 1 M NaCl electrolyte for the Ag/AgCl reference electrode. The counter-electrode was made of a 0.75 mm diameter platinum wire attached to a platinum foil disk. The disk was placed at the sealed end of the cell, and the wire was extended out through a tube. The working electrode consisted of 1 mm diameter platinum wire, 0.25 mm thick platinum foil, platinum wire gauze, and platinum black powder. The bent portion of the platinum strip, and the wire gauze disk, served to retain the platinum black powder in a near cylindrical configuration within the NMR coil.

Using this cell, these authors showed, for the first time, that NMR spectra could be observed within an electrochemical

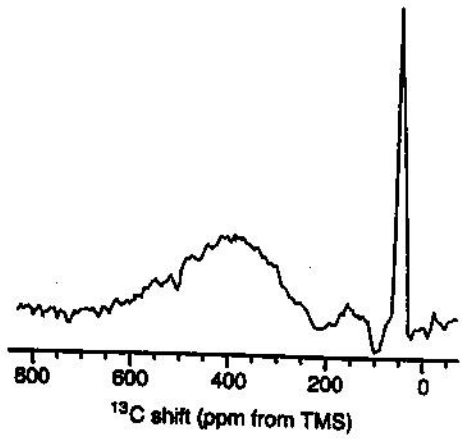

Fig. 1 The 7.05 T ^{13}C NMR spectrum of Pt ^{13}CO (ads) sample generated from 99% ^{13}C-enriched methanol decomposed on fuel cell grade platinum black powder, in 0.5 M H_2SO_4, 56 000 acquisitions, 0.25 s recycle delay, 500 Hz line broadening

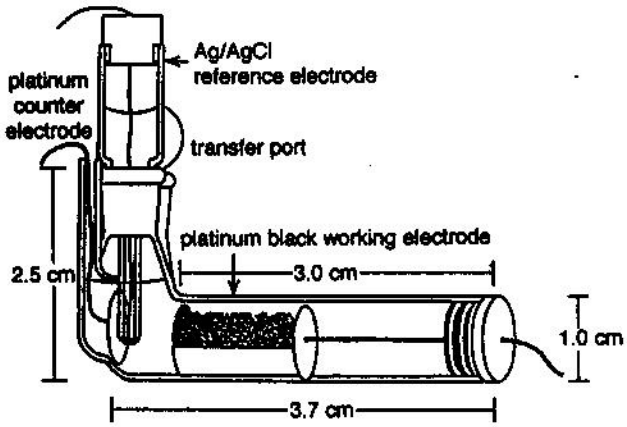

Fig. 2 Diagram of NMR electrochemical cell prototype. The fuel cell grade Pt-black powder is contained in a platinum foil boat.

cell, and the spectra observed were electrode potential dependent,[31,32] with the surface CO being stripped off the surface (as CO_2) at positive potentials.[32] However, there were severe limitations in the original design. The large number of acquisitions (*ca.* 10^5) needed in order to obtain a spectrum with an acceptable signal-to-noise ratio was prohibitive for detailed relaxation studies, and this led to our recent development of new probe designs and sample preparation methods, which we now discuss in more detail.

Sample preparation and spectroscopic aspects

We show in Fig. 3 a schematic of our new NMR electrochemical cell. The new cell was designed to permit both sample preparation and signal acquisition, avoiding sample transfer from a preparative electrochemical cell. That is, the sample can be generated and characterized *in situ* in the NMR magnet, without interruption of circuit continuity, immediately prior to performing the NMR measurements. The large electrolyte reservoir, which houses the counter and reference electrodes, provides ample electrolyte for complex and lengthy measurements to be made, without solvent evaporation. The location of the platinum black powder is within the long sample region of the cell. The sample cell is wrapped with a copper wire (the NMR coil) which serves for both excitation and signal acquisition, Fig. 3. The NMR electrochemical cell also incorporates the ability to exchange the electrolyte without removing the probe from the magnet. When directly connected to a potentiostat, use of the NMR electrochemical cell requires extensive electronic filtering of the electrochemical leads entering the probehead, in order to

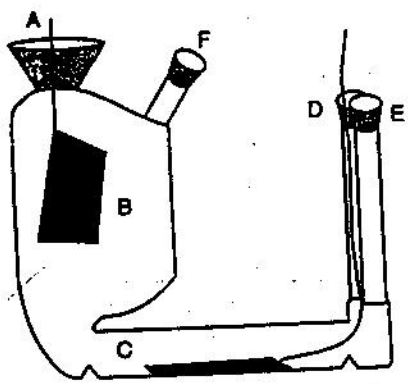

Fig. 3 Improved electrochemical NMR cell. A, platinum foil counter electrode, encased in a 14/20 male joint; B, upper electrolyte reservoir; C, sample chamber for Pt-black; D, working electrode lead connected to Pt gauze in sample chamber; E, vacuum/waste Luer connection; F, Ag/AgCl reference electrode Luer connection.

eliminate environmental radiofrequency pickup, as discussed in more detail below.

The NMR electrochemical cell is housed in the NMR probe, illustrated schematically in Fig. 4. The probe is designed for an 8.45 T (360 MHz) wide-bore (89 mm) superconducting magnet, and is loaded into the top of the magnet with the centre of the sample positioned at the magnetic centre. The electrochemical leads are connected to 0.141 inch diameter semi-rigid coax, which are part of the probe, by BNC connectors. The semi-rigid coax runs the length of the probe and enters into the probehead where the NMR electrochemical cell is located. Low-pass LC filters are installed at this point, as shown in Fig. 5 and in Table 1. These filters serve the dual purpose of minimizing the introduction of environmental noise, which can be transmitted through the electrochemical leads, plus they also act as rf chokes in the reverse direction, preventing the leakage of high-power excitation pulses out into the potentiostat. Typical circuit values for ^{13}C and ^{15}N NMR at 8.45 T are given in Table 1, and a typical time for obtaining a single spectrum from a ^{13}C sample at room temperature is 30 min (which is about the same as needed for an IR measurement of a common electrode adsorbate from smooth surfaces).

The techniques and equipment necessary for NMR signal acquisition are those typically used in solid-state NMR at the solid/gas interface. The frequency domain linewidths of typical ^{13}C or ^{15}N signals (^{13}CO, ^{13}CN, $C^{15}N$) on platinum at 8.45 T are *ca.* 20 kHz (full width at half maximum), requiring fast digitization for faithful reproduction of the rapidly decaying signal in the time domain (*ca.* 1 to 5 μs dwell times). At present, we are using the following equipment: for digitization, a Nicolet Explorer IIIA fast digitizer; for pulse control and data acquisition and Fourier transformation, a Nicolet 1280 computer system. Signal acquisition is accomplished by applying a Hahn spin-echo sequence followed by a signal acquisition period: [$\pi/2$–τ_e–π–τ_1–acquire], where $\tau_1 < \tau_e$ so that acquisition begins before the echo maximum. Typical values for τ_e are in the range of 25–40 μs. The precise echo maximum is located prior to Fourier transformation by left shifting the

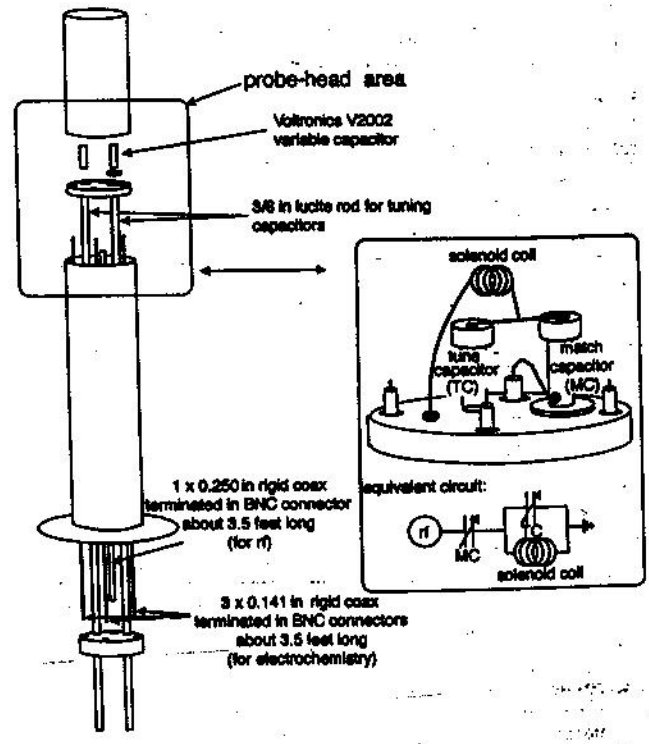

Fig. 4 Schematics of the NMR-electrochemistry probe and circuitry. The probe casing and cap are made of brass. All the internal pieces are made of copper.

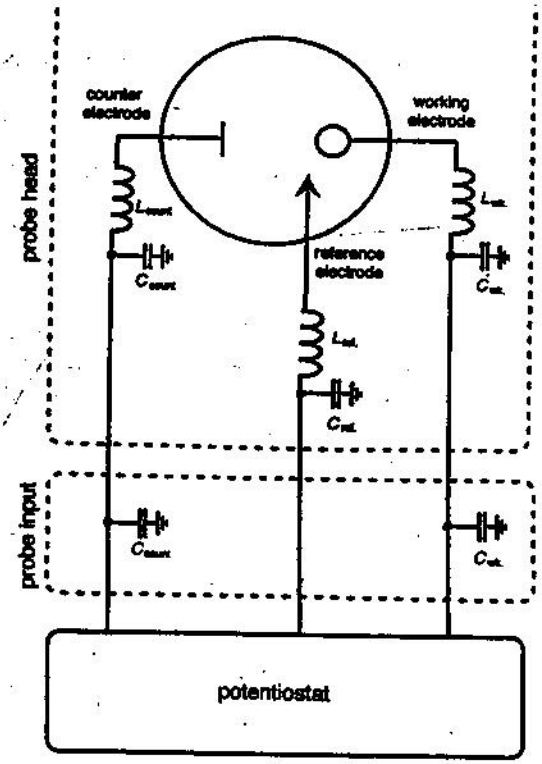

Fig. 5 Schematic of the low-pass filters used to enhance the signal-to-noise ratio and prevent excitation power from shunting out the electrochemical leads. The configurations of the tuning elements are listed in Table 1.

time-domain data. For low-temperature work, we use, at present, conventional sealed samples which are not under external potential control. A variety of sample sizes have been used and, in some sealed samples, we have diluted our samples with fine glass powder, which enhances rf penetration and thereby, sensitivity. The 90° pulse widths vary depending on sample size and nucleus under investigation, but are typically in the range 7–10 μs, with composite pulses being used to enhance the excitation band width.[33]

The fact that the echo decays very rapidly in the time domain leads to a problem common in solid-state NMR work: the appearance of a 'pulse feedthru'. This artifact results from the recovery of the receiver circuits and a ring-down of the transmitter and probe circuits after the high-power excitation pulses. To reduce this problem, a pulse sequence used to eliminate 'ringdown' in quadrupolar echo NMR was employed.[34] In this sequence, the phase of the $\pi/2$ and the π pulses of the Hahn echo sequence are varied such that the artifacts add destructively and are essentially eliminated, resulting in flat baselines.

Electrochemical adsorption and voltammetry

As noted above, we have used polycrystalline Pt-powder electrodes to help overcome the inherent sensitivity problems associated with surface NMR spectroscopy. Electrochemical adsorption is carried out in a three-electrode electrochemical cell, with a rolled platinum gauze as the counter electrode, and Ag/AgCl (1 M NaCl) as the reference electrode. In this cell, the platinum powder is evenly distributed over the Pt gauze, which is spot-welded to a platinum wire which is connected to a potentiostat. Prior to electrochemical adsorption of cyanide or CO from the electrochemical oxidation of MeOH, the Pt powder is chemically cleaned by soaking in warm chromic acid, then rinsed with Millipore water, and finally electrochemically cleaned by repeated cycling in 0.5 M sulfuric acid between −0.33 and 1.15 V, at a scan rate of 1 mV s^{-1}, until a regular voltammetric curve for clean platinum, Fig. 6A, is obtained.[35] For CN adsorption studies, the 0.5 M sulfuric acid solution is then replaced by a 0.5 M Na_2SO_4 solution, adjusted to pH 11.2 with sodium hydroxide. A vacuum is applied in order to speed up the rinsing–replacement procedure. The cyclic voltammogram (CV) curve in 0.5 M Na_2SO_4 is shown in Fig. 6B. A concentrated solution of ^{13}C-enriched sodium

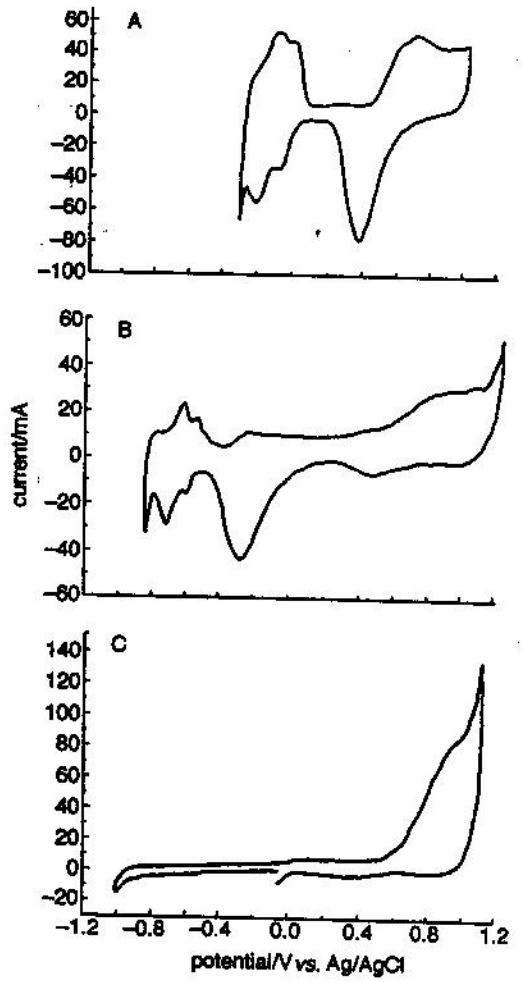

Fig. 6 CVs of Pt-powder electrodes, 1 mV s^{-1} scan rate. A, in 0.5 M H_2SO_4; B, in 0.5 M Na_2SO_4, pH 11.2; C, in 0.5 M Na_2SO_4, pH 11.2, pre-treated with $Na^{13}CN$ (0.2 M).

Table 1 Configuration of filter elements

	^{13}C (*ca.* 90.5 MHz)				^{15}N (*ca.* 36.5 MHz)			
	probehead		probe input		probehead		probe input	
electrodes	*L*/μH	*C*/pF	*L*/μH	*C*/pF	*L*/μH	*C*/pF	*L*/μH	*C*/pF
working	1.1	680	—	—	8.0	680	—	300
reference	1.1	680	—	—	11	—	—	—
counter	1.1	680	—	—	3.5	680	—	330

cyanide is then added to give a final concentration of 0.2 M CN^-, and adsorption carried out at −300 mV (*vs.* Ag/AgCl) until no current flow can be measured (*ca.* 1 h). When adsorption is complete, the solution containing excess cyanide is washed out using fresh deaerated 0.5 M Na_2SO_4 (pH 11.2) electrolyte. A basically similar procedure is used for MeOH electrodecomposition. Voltammetric characterization shows that the CN adsorbate results in a complete blocking of the Pt surface sites, Fig. 6C, and that there is no significant anodic current upon scanning up to +0.6 V (where platinum surface oxidation begins). However, holding the potential at 1.00 V for 30 min allows for oxidation of cyanide to cyanate (CNO^-) and/or carbonate (CO_3^{2-}),[36] and restores the surface to its original condition, as deduced from subsequent voltammetric profiles.

Surface NMR spectra

We have now obtained the ^{13}C NMR spectra of ^{13}CN and ^{13}CO (ex MeOH, ref. 29) electrochemically adsorbed onto polycrystalline fuel cell grade platinum (Johnson Matthey), as well as the ^{15}N NMR spectrum of $C^{15}N$ adsorbed onto the same material. Typical spectra are shown in Fig. 7. The ^{13}C spectra have similar line widths (full linewidths at half-height) of *ca.* 230 ppm, Fig. 7A, while the ^{15}N spectrum is somewhat broader, *ca.* 400 ppm, Fig. 7B. For ^{13}CO on Pt, the electrochemical cell results are quite similar in breadth and shift to those observed previously for CO from the gas phase on small supported-platinum particles, with frequency shifts of *ca.* 350 ppm from TMS being observed. ^{13}C NMR studies of CO on supported Pt in vacuum have shown that this large shift is to be ascribed to a Knight shift. The ^{13}CN shift is, however, much smaller, $\delta \approx 170$ ppm from TMS, implying a much smaller Knight shift. The observed lineshapes represent a combination of Knight shift anisotropies, chemical shift anisotropies, and broadening from magnetic field gradients from the Pt demagnetizing fields. As with the gas-phase systems, their detailed interpretation will require a future in depth theoretical analysis. However, in these gas-phase investigations, the NMR of surface atoms of metals has been observed[37] and already modelled phenomenologically.[38] The position of the surface Pt resonance has been derived from *ab initio* calculations,[39] and a local density formulation for the NMR parameters (Knight shift and T_1) has been applied for metals.[40] In addition, the electronic processes produced by chemisorption have also been addressed, *e.g.* ref. 41, although, overall, very few calculations are available for comparison with NMR data.[42] Fortunately, however, much detailed structural information can be deduced from relaxation measurements, in particular the spin–spin and spin–lattice relaxation times T_2 and T_1, and this will be the focus of the following sections, where we compare NMR-electrochemistry results for PtCN(ads) and PtCO(ads) with earlier studies of CO chemisorbed on supported Pt in vacuum.

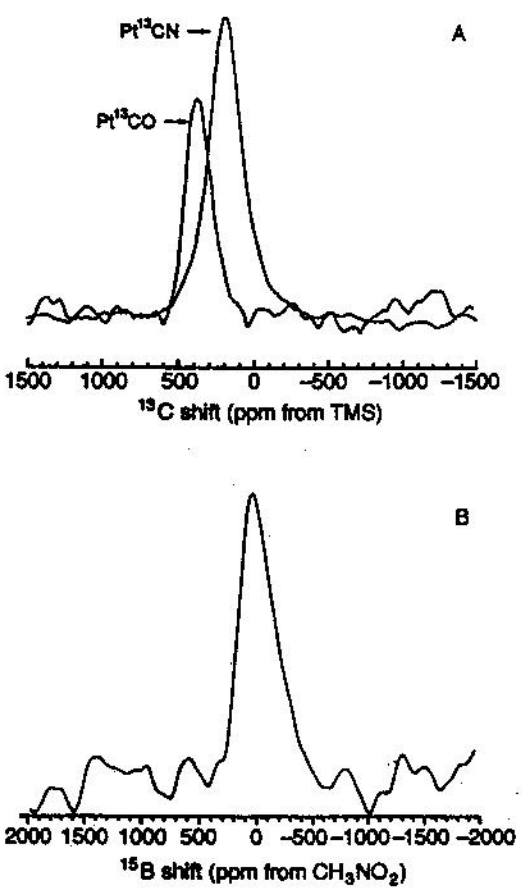

Fig. 7 The 8.45 T carbon-13 and nitrogen-15 surface spectra. A, $Pt^{13}CO$(ads) and $Pt^{13}CN$(ads). For $Pt^{13}CO$, in 0.5 M H_2SO_4, 13 200 acquisitions, 1 s recycle delay, 5000 Hz line-broadening, 1024 points; for $Pt^{13}CN$, in 0.5 M Na_2SO_4, pH 11.2, 5000 acquisitions, 1.5 s recycle delay, 5000 line-broadening, 2048 points. B, $PtC^{15}N$(ads), in 0.5 M Na_2SO_4, pH 11.2, 20 000 acquisitions, 2 s recycle delay, 5000 line-broadening, 2048 points.

Surface coverage and diffusion from T_2 measurements

In previous work, Slichter and co-workers have made extensive investigations of the spin–echo decay behaviour of ^{13}C nuclei in ^{13}CO adsorbed onto small supported metal catalyst particles[10,21,43] and, therefore, we begin our NMR-electrochemistry studies here using T_2 as a structural probe. When investigating samples under H_2O, there is clearly a possible problem associated with the presence of ^1H spins, which can contribute to a dipolar dephasing of the ^{13}C nuclei. This effect is shown in Fig. 8, where we present spin–echo-decay results for $Pt^{13}CN$(ads) and $Pt^{13}CO$(ads) in H_2O and D_2O. At 80 K, where ligand and water mobility is low, the presence of the abundant ^1H spins clearly causes a large enhancement in echo decay rate. However, this is effectively removed when a deuteriated electrolyte is employed, enabling an analysis of static structure using the methods previously employed for the supported catalysts in vacuum systems.[44,45] This approach is

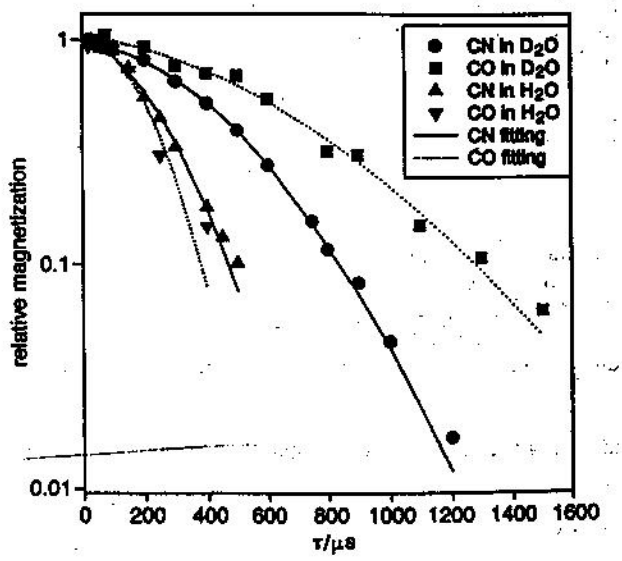

Fig. 8 T_2 decay results of $Pt^{13}CN$(ads) and $Pt^{13}CO$(ads) at 80 K in electrolyte with H_2O and D_2O as the solvent

simpler than implementing proton decoupling in our current instrument set-ups.

In the latter systems, the spin–echo decay was found to be produced by two mechanisms. The coupling of ^{13}C to the Pt spins produces a relaxation of Lorentzian character, with a characteristic time T_{2L}, as was shown previously by measurements with ^{13}CO diluted in ^{12}CO on supported Pt particles.[21] The other is the ^{13}C–^{13}C dipolar coupling which produces the so-called slow-beat of the spin–echo decay, from which information on C—C distances or clustering was obtained.[21] In cases where many neighbours in all spatial orientations are present, the slow beat can be approximated by a Gaussian with a time constant T_{2G}. Therefore, the spin–spin relaxation is expected to take the form:

$$M_{(t)} = M_{(0)} \exp[-(t/T_{2G})^2]\exp(-t/T_{2L})$$

Our relaxation curves are such that it is not possible to deduce from them both T_{2G} and T_{2L}, in large part because of limited sensitivity achievable with the Pt electrocatalysts at 8.45 T. We have therefore taken the value of T_{2L} measured independently of T_{2G} in the supported Pt system, namely 2.7 ms.[51] We believe this is a reasonable approach since this process is in the strong collision limit in which the relaxation time is equal to the correlation time (see below) and is independent of the strength of the coupling.

In order to get theoretical estimates for T_{2G} we have used the well known adlayer patterns on single crystal surfaces of CO to calculate the slow beat behaviour. Such patterns are similar or identical to those obtained from electrochemical adsorption of CO on single crystals.[46–48] Gas-phase T_{2G} is *ca.* 1.6 ms for a c(4 × 2) pattern on Pt(100), and 3.2 ms for a low CO coverage on Pt(100).[21] Hence, T_{2G} is very sensitive to the coverage. Our results for CO indicate that T_{2G} values are *ca.* 2.9 ms (31% coverage) and 2.1 ms (40% coverage) for decomposition times of 1 h at −150 mV and 4 h at 150 mV in deuteriated solvents, respectively. Thus, NMR measurements in an electrochemical environment permit a determination of coverage at the microscopic level which complements the electrochemical estimate. Such measurements could permit tests of possible local surface structure changes induced by an applied electric field. Of course, unlike diffraction methods, we cannot directly 'invert' our NMR data into a surface structure, although this can be done for bond lengths[21,22,26] with isolated pairs of nuclei.

The temperature dependence of T_2 is known to provide information on surface diffusion.[21,43,51] We show, in Fig. 9, the ^{13}C T_2 relaxation results of PtCO(ads) and PtCN(ads) samples in D_2O, as a function of temperature. For PtCO(ads), there is a minimum in T_2 at *ca.* 170 K. This occurs when the correlation time for CO motion is of the order of the reciprocal of the ^{13}C–^{13}C dipolar coupling, that is at the cross-over from the strong-collision to the weak-collision limit. Therefore, we account for the data using a simple model.[51] It involves two relaxation mechanisms: the fluctuations of the ^{13}C–^{13}C dipolar coupling by local motion of the adsorbate, and the random motion over the entire surface of the particle in the field gradient produced by the particle itself:

(1) a ^{13}C–^{13}C dipolar coupling with a splitting $\Delta\omega_1$;

(2) diffusion through a local magnetic field gradient, ΔH_{loc}, due to the magnetic polarization of the paramagnetic particles, producing a frequency change $\Delta\omega_2$;

(3) $1/T_2$ (other), to represent all other relaxation mechanisms, including the relaxation by Pt spin flips (which is a term proportional to temperature, see *e.g.* Fig. 2 of ref. 21).

There are also two motional regimes, the strong-collision limit, where:

$$\tau_c \gg \frac{1}{\Delta\omega}; \text{ where } \frac{1}{T_2} = \frac{1}{\tau}$$

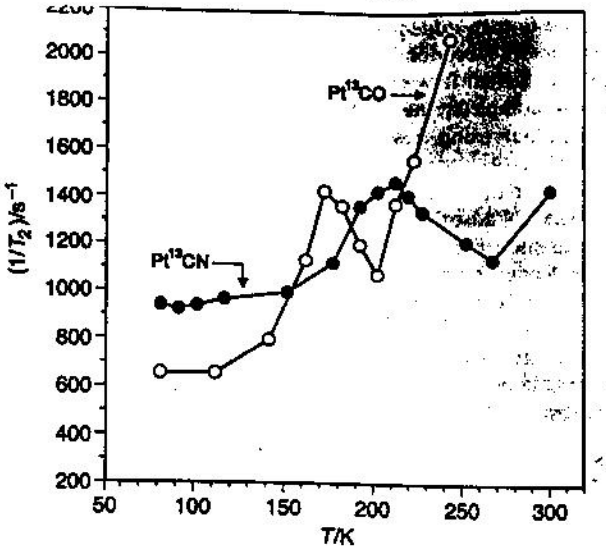

Fig. 9 Temperature dependence of spin–spin relaxation rate of Pt ^{13}CN (●) and $Pt^{13}CO$ (○) in deuteriated electrolyte

and the motional narrowing regime, where:

$$\tau_c \ll \frac{1}{\Delta\omega}; \frac{1}{T_2} = \Delta\omega^2\tau$$

For the dipolar interaction, the characteristic time τ_c is $\tau_c = \tau_{jump}$, while for diffusion over the Pt particle, $\tau_c = N^2\tau_{jump}$, where N is the number of jumps needed to travel over one quarter of the Pt surface circumference. The average jump time τ_{jump} is given by an Arrhenius relation:

$$\tau_{jump} = \tau_o \exp(E^*/k_B T)$$

where E^* is the activation energy.

This model accounts for the basic features of the temperature dependence of $1/T_2$ with: $\Delta\omega_1 = 1$ kHz, $\Delta\omega_2 = 25$ kHz, $N = 25$, $\tau_o = 1 \times 10^{-13}$ s, $E^* = 7.9$ kcal mole^{-1}, and $1/T_2(\text{other}) = 400\ s^{-1} + 4\ s^{-1}\ K^{-1}\ T$.[51]

These results obtained for CO on Pt in an electrochemical environment are quite close to those obtained previously for CO on a single crystal, and on supported-Pt catalysts in vacuum, where, in the latter case, an activation energy of 6.5 ± 0.5 kcal mol^{-1} was deduced from the time evolution of a half-flipped lineshape.[49] For CN on Pt, we see basically similar behaviour (Fig. 9). As with PtCO(ads), we again find a maximum in the $1/T_2$ relaxation rate, however, the activation energy increases from 8 ± 1 to 9 ± 1 kcal mol^{-1}, and the temperature of the $1/T_2$ maximum increases from *ca.* 170 to 205 K. Both values are larger than that of the CO adsorption, and are likely to be associated with stronger Pt–CN metal–adsorbate interactions, consistent with previous work.[50]

Towards electrocatalyst electronic structure from T_1

The spin–lattice relaxation of ^{13}CO on supported Pt in vacuum has been shown to be due to conduction electrons at the site of the C nucleus.[18,20] The strength of the relaxation depends on the nature of the bonding to the metal (extent of σ bonding and backbonding) and on the position of the energy levels relative to the Fermi level of the metal. Therefore, T_1 measurements give information on the bonding of the chemisorbate. Consequently, we have investigated the ^{13}C T_1 values for PtCO(ads) and for further comparison PtCN(ads), both in electrolyte solution. We show in Fig. 10A a typical inversion–recovery data set for $Pt^{13}CN$(ads), where we find that the data can be well fit to a single exponential, Fig. 10B. Similarly, we find a single-exponential recovery for PtCO(ads).[51] We have

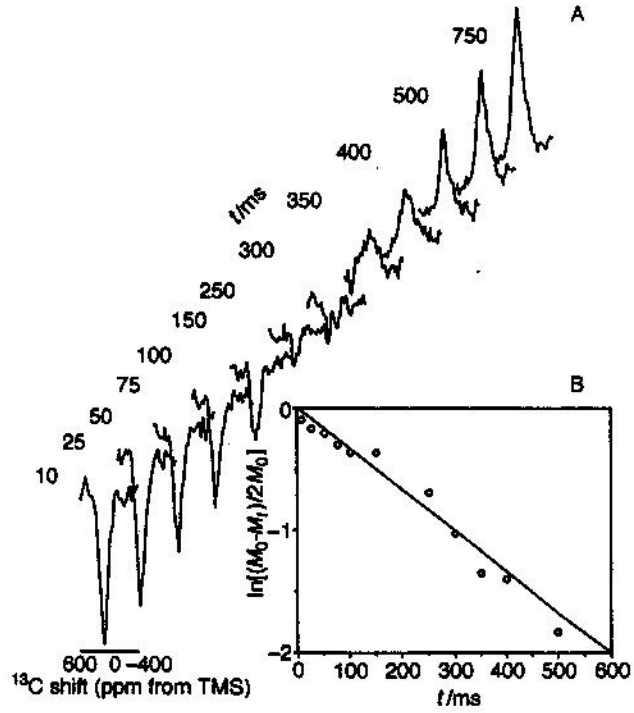

Fig. 10 Typical inversion–recovery spectra for $Pt^{13}CN(ads)$, A, and similar data fit to a single exponential, B

also been able to obtain ^{15}N T_1 relaxation data, although there is a substantial increase in the amount of acquisition time required, as expected on the basis of the small gyromagnetic ratio of ^{15}N. Interestingly, for all three systems, $Pt^{13}CN(ads)$, $PtC^{15}N(ads)$ and $Pt^{13}CO(ads)$, we find single exponential behaviour at temperatures where the adsorbates do not move on the NMR timescale, implying either a single site, or the presence of spin-diffusion. Since T_1T was not a function of temperature, we conclude the presence of a major, single site, in the electrochemical environment, as opposed to the two sites (terminal and μ_2-bridging) found in gas-phase studies of PtCO. We have also determined the spin–lattice relaxation times of each of these systems over a wide temperature range. In all three cases, we find that the spin–lattice relaxation rate is inversely proportional to temperature:

$$1/T_1 \propto T \text{ or } T_1T = \text{constant.}$$

Of all possible spin–lattice relaxation mechanisms, the observation that T_1T is constant is the hallmark of relaxation by conduction electron spins, or Korringa relaxation.[10,52] The strength of the relaxation mechanism implies that the conduction electrons are at the site of the nucleus.[20]

The smallest Korringa product is found for CO ex MeOH on Pt, where $T_1T = 80$ s K (Table 2), while the Korringa product for electrochemically adsorbed cyanide is *ca.* 135 s K at low temperatures, decreasing to *ca.* 90 s K at room temperature, Table 2. For the ^{15}N nucleus in PtCN(ads), we also find a complex temperature dependence of the Korringa product, as shown in Fig. 11. At low temperatures, $T_1T \approx 4000$ s K, while above *ca.* 200 K, $T_1T \approx 3000$ s K, as shown in Fig. 11. A similar decrease was observed in the T_1T product of ^{13}CO on supported Pd in vacuum,[53] and may indicate a small structural rearrangement.

Now, the spin–lattice relaxation induced by the contact hyperfine coupling is related to the Knight shift by the Korringa relation:

$$T_1T = \left(\frac{\hbar}{K^2 4\pi k_B}\right)\left(\frac{\gamma_e}{\gamma_n}\right)^2 B$$

Table 2 ^{13}CN and ^{13}CO spin–lattice relaxation data for sealed PtCN(aq) and PtCO(aq) samples (20% Pt) as a function of temperature, and a comparison between sealed sample and NMR electrochemical cell results

sample	temperature/K[a]	T_1/s[b]	T_1T/s K
20% $Pt/^{13}CN$ (sealed)	10	13.3	133
	12	11.5	138
	15	9.3	140
	20	7.1	142
	25	4.8	120
	33	4.1	135
	50	2.8	140
	77	1.5	116
	150	0.93	140
	200	0.68	136
	250	0.53	133
	298	0.3	89
100% Pt (sealed)	298	0.28	84
100% Pt (NMR electrochemical cell)	298	0.30	89
20% $Pt^{13}CO$ (sealed)	25	2.87	72
	50	1.59	80
	80	1.00	80
	110	0.72	79
	145	0.59	85
	180	0.45	81

[a] Accuracy is estimated to be *ca.* 1 K. [b] Accuracy is ±10%.

where K is the Knight shift, k_B is Boltzmann's constant and γ_n is the gyromagnetic ratio of the nucleus of interest. The greater ^{13}C T_1T product for CN than for CO is consistent with the ^{13}C NMR of CO having a greater Knight shift than CN. The much greater ^{15}N T_1T product is consistent with the idea that both CN and CO are directly bonded to Pt through carbon, since the strength of the relaxation depends on the probability for a conduction electron to be at the location of the nucleus. While a σ bond is expected to produce relaxation dominated by the contact hyperfine interaction and a Knight shift, π bonding can contribute to the relaxation only, *via* orbital and dipolar couplings. For example, with CN, the observed frequency shift is much less than might reasonably be expected from the Korringa relation, suggesting weak σ bonding. On the contrary, for CO, the T_1T of *ca.* 80 s K and the Korringa relation yield a Knight shift of *ca.* 230 ppm, which translates to a total shift from TMS of *ca.* (230 + 165) = 395 ppm downfield from TMS, quite close to the $\delta \approx 350$ ppm we observe experimentally. Ultimately, such considerations have the potential to provide considerable information on the electronic properties of the interface.[54] For example, they could provide insights, from an electronic point

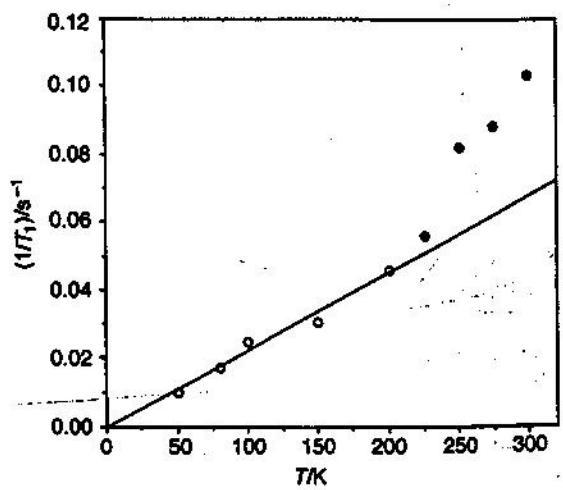

Fig. 11 Temperature dependence of the spin–lattice relaxation rate as a function of temperature for $C^{15}N$ on Pt

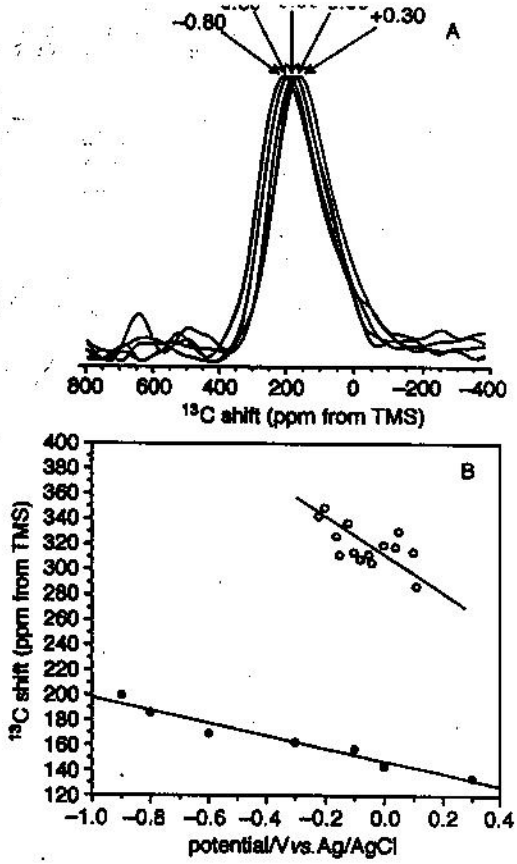

Fig. 12 A, ^{13}C NMR spectra of Pt^{13}CN(ads) as a function of applied potential. Each spectrum was obtained using 5000 acquisitions, a 1.5 s recycle delay, 1000 Hz line-broadening, 2048 points. B, ^{13}C chemical shift *vs.* potential for Pt^{13}CN(ads) (●) and Pt^{13}CO(ads) (○).

of view, into the differences in the bonding of CO to Pt which have been observed between UHV and solution spectroscopic studies,[55–63] where Weaver and co-workers[61,62] have shown that the surface potential for platinum in an electrochemical cell is *ca.* 1 V lower than in UHV. As a consequence, while the metal–CO back donation to the 2π orbital in an electrochemical environment is enhanced, donation from the CO 5σ is retarded, and a weakening of the metal–CO bond occurs. Comparison of CO on Pt in an electrolyte and under vacuum conditions is of course complicated by the presence, in the latter case, of several sites having different T_1T products,

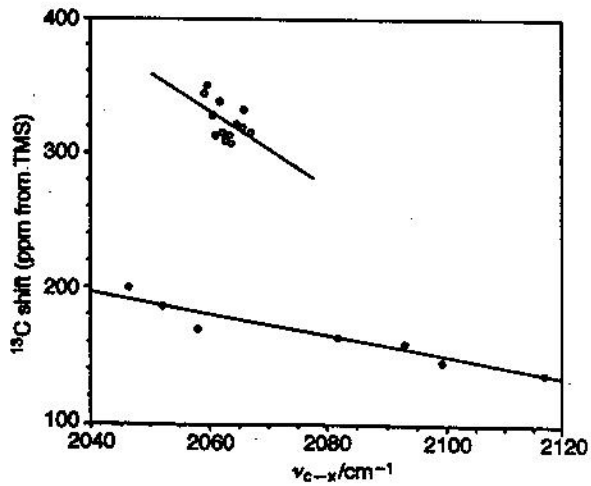

Fig. 13 ^{13}C NMR chemical shift of CN (●) and CO (○) on Pt *vs.* IR frequency, as a function of applied potential

ranging from 20 to 400 s K, but once firm gas-phase assignments are in hand, comparison with the NMR-electrochemistry results can be readily made.

We now move to consider the final topic of this article, the observation of electric-field induced effects in the spectra from electrochemical samples.

Electrostatic field effects on NMR spectra

Electric fields at the electrode/electrolyte interface are known to be very large, of the order of $(1–3) \times 10^7$ V cm^{-1}.[64,65] Indeed, the effects of these enormous fields at the electrode/electrolyte interface are, in a sense, the essence of electrochemistry.[64] It is, therefore, highly desirable to try to develop new techniques to probe these fields, including how they might, for example, modify the electronic structure and interactions of species reacting at electrodes.

We have begun, therefore, to study the effects of potential control on NMR observables in the PtCN(ads) and PtCO(ads) systems, and typical spectra for ^{13}CN adsorbed on a Pt electrode as a function of applied potential are shown in Fig. 12. These results are of some interest since they represent the first observation of NMR frequency shifts due to electric fields in an electrochemical cell. Related 'Stark tuning' shifts have of course been observed previously in the IR,[66,67] and we can utilize these earlier results to obtain the NMR–IR correlations shown in Fig. 13.

For ^{13}CN, we are able to investigate a large range of applied potentials, and we obtain a reasonably accurate vibrational shielding derivative, $\delta\sigma/\delta\nu$, of −0.81 ppm cm^{-1} (Fig. 13). For ^{13}CO, a much smaller range of applied potentials is accessible (before CO oxidation). There is, therefore, more scatter in the data, a problem which we believe will be substantially alleviated in the future by working at higher magnetic field strengths where sensitivity will be enhanced. For ^{13}CO, the vibrational shielding derivative is *ca.* −2.8 ppm cm^{-1}.

In both cases, we find that the ^{13}C resonances become more shielded on application of a more positive applied potential. This is the response which is to be expected if both CN and CO have C directly attached to platinum, although the complexities associated with the presence of conduction electrons will need to be carefully addressed in future work, using *e.g.* density functional theory on large Pt clusters (treated using effective core potentials).[68,69] Careful NMR investigations of shift and spin–lattice relaxation rates as a function of applied potential could help resolve the controversy as to whether the effect of the electric field is a Stark effect, or is to be ascribed to charge transfer.[70] At this point, we can state that we do see responses of the NMR resonances to applied electric fields, and it is of interest that the experimental NMR/IR vibrational shielding derivatives we see are of the same sign for both PtCN(ads) and PtCO(ads) (Fig. 13). In the future, it is likely that each of the other NMR observables we have discussed above: T_1, T_2, ΔE^*, $T(T_2 \text{ min})$, will also be susceptible to the effects of *E*-fields. For example, if CN is stabilized by an applied *E*-field, then we expect that the activation barrier to diffusion, as well as the temperature of the T_2 min, will reflect this in a readily interpretable way. Also, of course, it may be possible to detect the effects of *E*-fields on the electronic densities of states from Knight shifts and T_1T results, although this is a more challenging proposition, for both theory and experiment.

Future prospects

The results we have presented above represent the first detailed foray into the new field of electrochemical NMR. Our results indicate that surface NMR resonances can be observed in an electrochemical environment, and under potential

control. To date, we have obtained variable-temperature T_1 and T_2 results on ^{13}C and ^{15}N spins. Sensitivity at 8.45 T (corresponding to a 360 MHz ^1H NMR resonance frequency) is only moderate, but will be enhanced considerably in the near future with the use of a novel multiple-probe 600 MHz spectrometer, which will enable investigation of two electrochemical samples, simultaneously.[71] In the future, many other nuclei of interest in electrochemistry/electrocatalysis can also be investigated, *e.g.* ^1H, ^{17}O, ^{19}F, ^{27}Al, ^{31}P, ^{195}Pt, and $^{203,205}Tl$. It should be possible to observe *e.g.* surface and subsurface Pt and hydrogen, to investigate anion chemisorption processes on metal electrodes *via e.g.* ^{31}P NMR of adsorbed phosphate, to use ^{27}Al NMR to investigate aluminium corrosion science, essentially everything which has been investigated in analogous gas-phase/heterogeneous catalysis/solid-state NMR should now be accessible *via* the NMR-electrochemistry approach, and the reader is referred to several reviews of the basic scope of NMR in heterogeneous catalysis for further details.[9–12,72]

NMR is, in a sense, unique in its ability to probe static structure (bond lengths, bond angles, surface geometries), dynamic structure (diffusion from T_2 and lineshape, as well as internal rates and types of motion), and electronic structure (from chemical shifts, shift tensors, Knight shifts, electric field gradients). In the presence of strong electric fields, each of these parameters can be expected to respond due to polarization of the orbital or conduction electrons. The results we have presented in this article open up broad new areas in electrochemical surface science, since we have now shown that it is possible to perform many conventional solid-state NMR experiments in an electrochemical environment. Since electrochemistry provides a means of cleaning surfaces at much lower temperatures than those used for supported catalysts, samples of much greater overall metallic surface area can be used in NMR-electrochemistry than can be obtained for NMR studies of heterogeneous, gas-phase catalysts. Hence, NMR-electrochemistry methods will, hopefully, soon become a valuable new tool for electrocatalysis surface science.

This work was supported by the United States National Science Foundation Material Research Laboratory Program (grant NSF DMR 89-20538 to E.O.), by the United States Department of Energy (grant DE-AC02-76ER01198 to A.W.), and the National Science Foundation (grant CHE-11184 to A.W.), by the Aluminum Neuhausen Fund of the Swiss Federal Institute of Technology (grant 204 to P.A.V.), and in part by the United States National Institute of Health (grant HL-1948 to E.O.). A.W. acknowledges an isotope grant from Cambridge Isotope Laboratories, Inc., Cambridge, MA.

References

1 M. Mehring, *Principles of High Resolution NMR in Solids*, Springer, New York, 1983.
2 C. P. Slichter, *Surf Sci.*, 1981, **106**, 382.
3 C. P. Slichter, *Annu. Rev. Phys. Chem.*, 1986, **37**, 25.
4 J. P. Burger, N. J. Poulis and W. P. A. Haas, *Physica*, 1961, **27**, 514.
5 T. Ito, T. Kadowski and T. Toya, *Jpn. J. Appl. Phys.*, 1974, Suppl. 2, Part 2, p. 257.
6 T. Ito and T. Kadowski, *Jpn. J. Appl. Phys.*, 1975, **14**, 1673.
7 T. Ito, T. Kumagai and T. Kadowski, *Jpn. J. Appl. Phys.*, 1977, **16**, 1919.
8 H. Pfeifer, in *NMR Basic Principles and Progress*, ed. P. Diehl, E. Fluck and R. Kosfeld, Springer, Berlin, 1972, vol. 7, p. 53.
9 T. M. Duncan and C. Dybowski, *Surf Sci. Rep*, 1981, **1**, 157.
10 J-Ph. Ansermet, C. P. Slichter and J. H. Sinfelt, *Prog. NMR Spectrosc.*, 1990, **22**, 401.
11 P. K. Wang, J-Ph. Ansermet, S. L. Rudaz, Z. Wang, S. Shore, C. P. Slichter and J. H. Sinfelt, *Science*, 1986, **234**, 35.
12 T. M. Duncan, *Colloids Surf.*, 1990, **45**, 11.
13 T. M. Duncan, J. T. Yates Jr. and R. W. Vaughan, *J. Chem. Phys.*, 1980, **73**, 975.
14 T. M. Duncan and T. W. Root, *J. Phys. Chem.*, 1988, **92**, 4426.
15 T. M. Duncan, A. M. Thayer and T. W. Root, *J. Chem. Phys.*, 1990, **92**, 2663.
16 T. M. Duncan, A. M. Thayer and T. W. Root, *Phys. Rev. Lett.*, 1989, **63**, 62.
17 L. R. Becerra, C. P. Slichter and J. H. Sinfelt, *J. Phys. Chem.*, 1993, **97**, 10.
18 S. L. Rudaz, J-Ph. Ansermet, P. K. Wang, C. P. Slichter and J. H. Sinfelt, *Phys. Rev. Lett.*, 1985, **54**, 71.
19 P. K. Wang, J-Ph. Ansermet, C. P. Slichter and J. H. Sinfelt, *Phys. Rev. Lett.*, 1985, **55**, 2731.
20 J-Ph. Ansermet, P. K. Wang, C. P. Slichter and J. H. Sinfelt, *Phys. Rev. B*, 1988, **37**, 1417.
21 J-Ph. Ansermet, C. P. Slichter and J. H. Sinfelt, *J. Chem. Phys.*, 1988, **88**, 5963.
22 S. E. Shore, J-Ph. Ansermet, C. P. Slichter and J. H. Sinfelt, *Phys. Rev. Lett.*, 1987, **58**, 953.
23 T. M. Duncan, K. W. Zilm, D. M. Hamilton and T. W. Root, *J. Phys. Chem.*, 1989, **93**, 2583.
24 K. W. Zilm, L. Bonneviot, D. M. Hamilton, G. G. Webb and G. L. Haller, *J. Phys. Chem.*, 1990, **94**, 1463.
25 P. K. Wang, Ph.D. Thesis, University of Illinois at Urbana-Champaign, 1984.
26 P. K. Wang, C. P. Slichter and J. H. Sinfelt, *Phys. Rev. Lett.*, 1984, **53**, 82.
27 P. K. Wang, C. P. Slichter and J. H. Sinfelt, *J. Phys. Chem.*, 1990, **94**, 1154.
28 A. Wieckowski, S. D. Rosasco, G. N. Salaita, A. T. Hubbard, B. Bent, F. Zaera, D. Godbey and G. A. Somorjai, *J. Am. Chem. Soc.*, 1985, **111**, 7653.
29 K. W. H. Chan and A. Wieckowski, *J. Electrochem. Soc.*, 1990, **137**, 367.
30 P. J. Slezak and A. Wieckowski, *J. Electroanal. Chem.*, 1992, **339**, 401.
31 P. J. Slezak and A. Wieckowski, *J. Magn. Reson. A*, 1993, **102**, 166.
32 P. J. Slezak, Ph.D. Thesis, University of Illinois at Urbana-Champaign, 1992.
33 R. R. Ernst, G. Bodenhausen and A. Wokaun, *Principles of Nuclear Magnetic Resonance in One and Two Dimensions*, Oxford University Press, 1987.
34 A. C. Kunwar, G. L. Turner and E. Oldfield, *J. Magn. Reson.*, 1986, **69**, 124.
35 H. Angerstein-Kozlowska, B. E. Conway and W. B. A. Sharp, *J. Electroanal. Chem.*, 1973, **43**, 9.
36 H. Tamura, T. Arikado, H. Yoneyama and Y. Matsuda, *Electrochim. Acta*, 1974, **19**, 272.
37 C. D. Makowka, C. P. Slichter and J. H. Sinfelt, *Phys. Rev. Lett.*, 1982, **49**, 379; J. J. van der Klink, J. Buttet and M. Graetzel, *Phys. Rev. B*, 1984, **29**, 6352.
38 C. D. Makowka, C. P. Slichter and J. H. Sinfelt, *Phys. Rev. B*, 1985, **31**, 5663; J. P. Bucher and J. J. van der Klink, *Phys. Rev. B*, 1988, **38**, 11038.
39 M. Weinert and A. J. Freeman, *Phys. Rev. B*, 1983, **28**, 6262.
40 J. J. van der Klink, *J. Phys.: Condens. Matter*, 1996, **8**, 1845.
41 R. Hofmann, *Rev. Mod. Phys.*, 1988, **60**, 601; P. Felbelman and D. R. Hamann, *Surf. Sci.*, 1985, **149**, 48.
42 J. Andzelm and D. R. Salahub, *Int. J. Quantum Chem.*, 1986, **29**, 1091.
43 J-Ph. Ansermet, Ph.D. Thesis, University of Illinois at Urbana-Champaign, 1985.
44 D. B. Zax, C. A. Klug, C. P. Slichter and J. H. Sinfelt, *J. Phys. Chem.*, 1989, **93**, 5009.
45 C. A. Klug, C. P. Slichter and J. H. Sinfelt, *J. Phys. Chem.*, 1991, **95**, 2119.
46 D. Zurawski, M. Wasberg and A. Wieckowski, *J. Phys. Chem.*, 1990, **94**, 2076.
47 C. K. Rhee, J. M. Feliu, E. Herrero, P. Mrozek and A. Wieckowski, *J. Phys. Chem.*, 1993, **97**, 9730.
48 I. Oda, J. Inukai and M. Ito, *Chem. Phys. Lett.*, 1993, **203**, 99.
49 L. R. Becerra, C. A. Klug, C. P. Slichter and J. H. Sinfelt, *J. Phys. Chem.*, 1993, **97**, 12014.
50 P. Zelenay and A. Wieckowski, in *Electrochemical Interfaces: Modern Techniques for In-Situ Interface Characterization*, ed. H. D. Abruña, VCH, New York, 1991, p. 479.
51 J. Day, P. A. Vuissoz, E. Oldfield, A. Wieckowski and J-Ph. Ansermet, *J. Am. Chem. Soc.*, 1996, **118**, 13046.
52 C. P. Slichter, *Principles of Magnetic Resonance*, Springer-Verlag, New York, 1990, p.156.
53 S. E. Shore, Ph.D. Thesis, University of Illinois at Urbana-Champaign, 1986.

54 Y. Y. Tong, G. A. Martin and J. J. van der Klink, *J. Phys. Condens. Matter*, 1994, **6**, L533.
55 G. Blyholder, *J. Phys. Chem.*, 1964, **68**, 2772.
56 J. N. Miller, I. Lindau and W. E. Spicer, *Surf. Sci.*, 1981, **111**, 595.
57 E. W. Plummer and W. Eberhardt, in *Angle-Resolved Photoemission as a Tool for the Study of Surface*, ed. I. Prigogine and S. A. Rice, *Advances in Chemical Physics*, Wiley, New York, 1982, vol. 49.
58 K. R. Nabe and A. B. Anderson, *Surf. Sci.*, 1982, **119**, 35.
59 M. Trenary, S. L. Tang, R. J. Simonson and F. R. McFeely, *Surf. Sci.*, 1983, **124**, 555.
60 J. Rogozik and V. Dose, *Surf. Sci.*, 1986, **176**, L847.
61 S. C. Chang, L. W. H. Leung and M. J. Weaver, *J. Phys. Chem.*, 1989, **93**, 5341.
62 S. C. Chang and M. J. Weaver, *Surf. Sci.*, 1990, **238**, 142.
63 Y. T. Wong and R. Hoffmann, *J. Phys. Chem.*, 1991, **95**, 859.
64 J. O'M. Bockris and A. K. N. Reddy, *Modern Electrochemistry*, Plenum, New York, 1970.
65 C. Korzeniewski, S. Pons, P. P. Schmidt and M. W. Severson, *J. Chem. Phys.*, 1986, **85**, 4153.
66 C. Stuhlmann, I. Villegas and M. J. Weaver, *Chem. Phys. Lett.*, 1994, **219**, 319.
67 P. S. Bagus, C. J. Nelin, W. Muller, M. R. Philpott and H. Seki, *Phys. Rev. Lett.*, 1987, **58**, 559.
68 M. F. Baba, C. Mijoule, N. Godbout and D. R. Salahub, *Surf. Sci.*, 1994, **316**, 349.
69 C. Bureau, M. Defranceschi, J. Delhalle, G. Lecayon and D. R. Salahub, *J. Mol. Struct. (Theochem.)*, 1995, **330**, 279.
70 R. J. Nichols, in *Adsorption of Molecules at Metal Electrode*, ed. J. Lipkowski and P. N. Ross, VCH, Weinheim, 1992, p. 347.
71 E. Oldfield, *J. Magn. Reson. A*, 1994, **107**, 255.
72 *NMR Techniques in Catalysis*, ed. A. T. Bell and A. Pines, Dekker, New York, 1994.

Paper 6/03611B; *Received* 23*rd May*, 1996